Available online at www.sciencedirect.com
SCIENCE DIRECT®
Journal of Power Sources 145 (2005) 362–368
JOURNAL OF POWER SOURCES
www.elsevier.com/locate/jpowsour

Stainless steel bipolar plates

Shuo-Jen Lee*, Jian-Jang Lai, Ching-Han Huang

Department of Mechanical Engineering, Yuan Ze University, 135 FarEast Road, NeiLi, TaoYuan, Taiwan, ROC

Accepted 10 January 2005
Available online 22 April 2005

Abstract

In this research, a specific surface modification technology was developed for stainless steel bipolar plates to obtain a corrosion-resistant oxide film. The surface roughness was measured, and an electron spectroscopy analysis (ESCA) was conducted to verify the chemical composition of the surface layer. From the binding energy of the ESCA spectrum, the amounts of chemical shift were used to identify the major chemical compositions. The thickness of the oxide film was analyzed by auger electron spectroscopy (AES). From the results of the ESCA and AES analyses, the effects of the surface modification on the integrity of the surface were evaluated. Uniform corrosion and localized corrosion tests were also conducted to investigate any improvement on the corrosion characteristics. A single cell was assembled for cell performance tests.

The surface of the treated plates was bright and smooth. The ESCA and AES analyses showed that the treated plates had a much higher chrome content. The metallurgical structure was dense with substantially less defects. The chemical and electrochemical properties were more stable. The corrosion rates of the treated plates were also much improved, resulting in better electric conductivity, stable cell performance as well as longer cell life.

Keywords: Electrochemical process; Stainless steel; Fuel cell; Surface integrity; Metallic corrosion

1. Introduction

When it comes to the proton exchange membrane fuel cell (PEMFC), the area of metallic bipolar plates is attracting a lot of research activities. One of the popular trends is to adopt corrosion-resistant materials such as stainless steel and titanium. Usually the density of these materials is higher, leading to a heavier stacking assembly. The other trend is to use light metal such as aluminum, coated with corrosion-resistant film, as the substrate material. To date, some commercial prototypes of stationary fuel cell systems utilizing stainless steel bipolar plates have been produced. However, the naturally formed oxide layer of stainless steel had a loose structure, contains inclusions, contaminants and oil stains. Its thickness is substantial, and the conductivity is poor. The Fe ions may dissolve more easily in an acidic environment which will result in MEA poison.

Hornung and Kappelt [1] studied Fe-based alloys for use as bipolar plates, and found that the corrosion rates of the gold-plated Ni-based alloys were similar to those of Fe-based alloys. However, gold-plated bipolar plates had a better electrical conductivity. Davies et al. [2] adopted different stainless steels including SS316L, SS310 and SS904L for their gold-plated Ni-based alloys. The oxide film of stainless steel has good corrosion resistant capability. The thicker the oxide film the better the corrosion resistance. However, it also reduces conductivity. The higher contents of Cr and Ni in the stainless steel result in a thinner oxide film and better cell performance. Therefore, the performance of the cell were rated SS316L < SS310 < SS904L. Wang et al. [3] studied the characteristics of Cr contained in stainless steels. The results showed that the surface properties became more stable with the increase in Cr content. The Cr contents were rated SS349^{TM} > SS904L > SS317L > SS316L, which was the same as the corrosion rate. The results of both Davies and Wang verified the importance of Cr content in stainless steel used for metallic bipolar plates.

* Corresponding author. Tel.: +886 3 4648800; fax: +886 3 4558013.
E-mail address: mesjl@saturn.yzu.edu.tw (S.-J. Lee).

0378-7753/$ – see front matter © 2005 Elsevier B.V. All rights reserved.
doi:10.1016/j.jpowsour.2005.01.082

In this study, an electrochemical process was employed for the surface modification of stainless steel in order to demonstrate its feasibility for use in PEM fuel cells. The chemical compositions, metallurgical structure, film thickness and morphology of the surface layer were altered by this electrochemical process. The effects on surface roughness, corrosion resistance, contact resistance and cell performance were tested and compared for evaluation.

2. Specimen material and experimental procedures

SS316L (ASTM) was selected as the specimen material. It is widely used in the biomedical and electronic industries to meet stringent cleanliness and high corrosion resistant requirements. The sizes of the work specimens were 90 mm × 90 mm × 3 mm, respectively, cut from commercially available cold-rolled plates.

The experimental procedures are listed in Fig. 1. First, the flow fields may be fabricated by computer numerical control (CNC), electrical discharged machining (EDM) or electrochemical machining (ECM). The plates were then lightly ground on the top surface to ensure flatness. The plates were then degreased in an organic solvent, ultrasonically cleaned in an alkaline liquid for the purpose of neutralization, followed by, immersion in nitride, then a final ultrasonic cleaning in de-ionized water and final drying, before starting the surface treatment by electrochemical process.

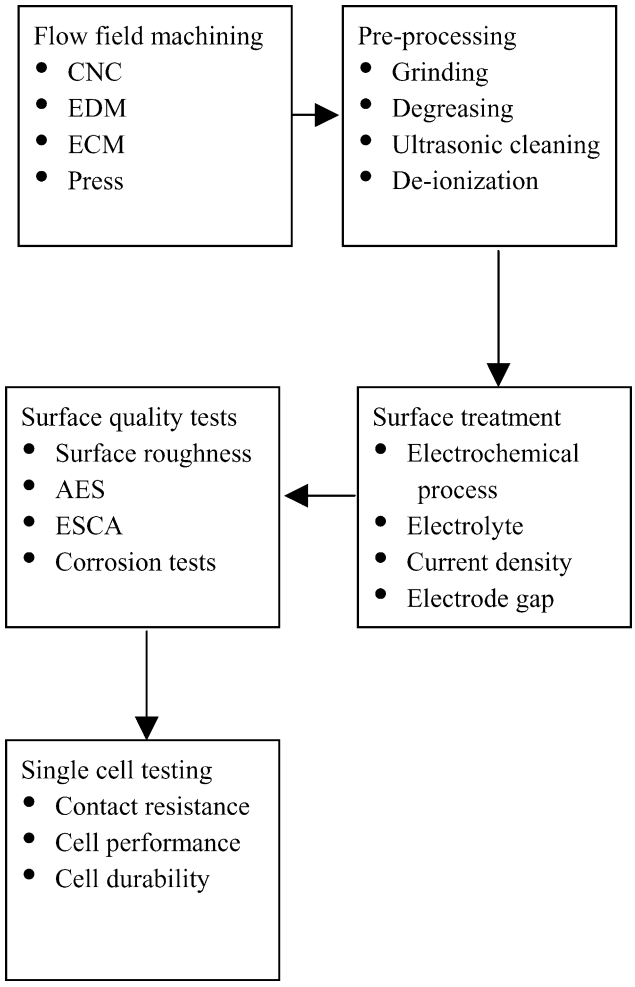

Fig. 1. Schematic plot of experimental procedures.

The salient parameters for the electrochemical process were the compositions of electrolyte, the operating current density, the operating voltage, the processing time and the gap between the electrodes [4]. A simple experimental design of the above variables was designed for four tests in order to compare their effects on the surface integrity of the processed specimen.

The processed specimens were tested for surface roughness of the improvement in surface morphology. electron spectroscopy analysis (ESCA) was used to verify the changes in chemical compositions of the surface film. The thickness of the surface film was analyzed by auger electron spectroscopy (AES). A thicker oxide film may have a longer anti-corrosion life, but the surface conductivity will be lower. Consequently, a thin but dense oxide film is preferred. The corrosion resistant capability was tested with the uniform corrosion test and the pitting potential analysis. The corrosion rate was evaluated by the uniform corrosion test. It must be noted that the pitting potential analysis is also important in evaluating localized corrosion characteristics which may the source for metallic ion poison.

Finally, the contact resistance under various stacking pressures was measured for these four processed specimens. The proper stacking pressure for the single cell was then evaluated. Single cells for these four processed stainless steel bipolar plates were assembled and underwent a cell performance test and compared with graphite and the original SS316L plates.

3. Experiments and their results

Many factors may affect cell performance and cell life, such as MEA characteristics, bipolar plate performance, stacking and operating parameters. In the following experiments, surface integrity tests and cell performance tests were carried out, and the results compared, after the electrochemical process was conducted.

3.1. Surface morphology property—surface roughness measurements

The surface roughness creates minute potential differences between the peaks and the valleys in the electrochemical environment. The peaks have a stronger electric potential which leads to a more rapid dissolution of the metallic ions. The proposed electrochemical process may improve the surface roughness by this smoothing and leveling electrochemical reaction.

Table 1
Surface roughness of various process specimens

Test no.	Original specimen	Processed specimen 1	Processed specimen 2	Processed specimen 3	Processed specimen 4
R_{max} (μm)	1.3	0.8	0.3	0.4	0.6
R_a (μm)	0.115	0.084	0.034	0.045	0.058

The roughness values of the original plates are listed in Table 1. They are R_a 0.115 μm and R_{max} 1.3 μm. The morphology under optical microscopy is shown in Fig. 2a. It has rolling marks, inclusions and micro-cracks. Fig. 2b shows the surface reflection of the plate, which is blurry and dull.

Four tests with different process parameters were conducted. The R_a and R_{max} values of the original and processed specimens were measured. Their values are listed in Table 1. Specimen 1 did not have sufficient processing time, and as a result the values of the surface roughness were higher and not very uniform, and the surface reflection was dull. Specimen 2 showed the best result. The R_{max} and R_a values were reduced to 0.3 and 0.034 μm, respectively, a significant three to four-fold improvement. The pictures by optical microscopy of the surface morphology and the surface reflection are shown in Fig. 3a and b. They are smooth and bright. The lettering of the ruler could be seen clearly from the reflection. Specimens 3 and 4 also show good improvement compared with the original plates. In specimen 3, the sharp edges of the original plates were rounded-off, but this may be due to the longer processing time.

From the results of Tables 1 and 4, it is evident that the electrochemical processing parameters have a great effect on the surface quality. It is also evident that proper control and selection of these parameters is important. Except for specimen 1, specimens 2–4 all had a two- to four-fold improvement in surface roughness. Comparing Fig. 2a with 3a, surface defects were mostly removed. The structure looked dense and smooth.

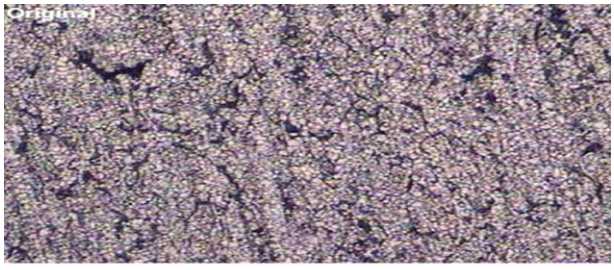

(a)

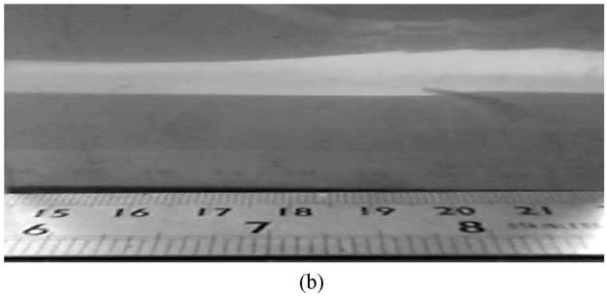

(b)

Fig. 2. (a) Optical microscopy (×50). (b) Dull surface reflection.

3.2. Chemical compositions of the surface film—ESCA and AES analyses

The chemical compositions of the surface film were analyzed by ESCA. From the ESCA spectrum, the binding energy was compared with the data bank to identify the amount of chemical shift and the chemical compositions of the elements [5]. The results are listed in Table 2. The Cr/Fe ratio increased from the original value of 0.51 to between 0.72 (specimen 1) and 2.01 (specimen 2). Taking specimen 2 as an example, the Cr content increased from 26.88% to 57.23%. At the same time, the Fe content reduced from 52.40% to 28.43%. The content of the oxide film had changed from the dominating Fe_2O_3 to mostly Cr_2O_3. Chrome oxide is stable in an acidic environment such as the PEM fuel cells, while Fe_2O_3 will dissolve. Thus, the increase in Cr content will increase the corrosion resistance and chemical stability. The reduction in Fe content will decrease the dissolution of Fe ions and thus reduce the MEA poisoning by Fe ions.

The AES depth profile analysis provides the changes in the metallurgical composition at different depths [5]. Table 3 shows the depth of the oxide film for each specimen. The

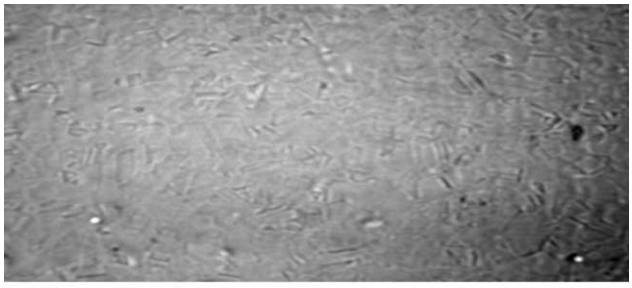

(a)

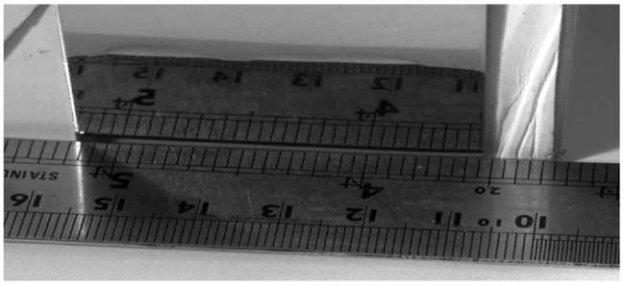

(b)

Fig. 3. (a) Observation of specimen 2 by optical microscopy (×50). (b) Mirror-like surface reflection of specimen 2.

Table 2
Cr/Fe ratio of the oxide film by ESCA analysis

Test no.	Original specimen	Processed specimen 1	Processed specimen 2	Processed specimen 3	Processed specimen 4
Cr (%)	26.88	34.11	57.24	51.23	47.34
Fe (%)	52.40	47.64	28.43	28.12	33.76
Cr/Fe ratio	0.51	0.72	2.01	1.82	1.40

Table 3
Thickness of the oxide film by AES analysis

Test no.	Original specimen	Processed specimen 1	Processed specimen 2	Processed specimen 3	Processed specimen 4
Depth (Å)	47.7	38.6	25.8	26.7	27.8

original plate is shown to have the thickest oxide film, 47.7 Å. However, judging from Fig. 2a, its structure was loose with a lot of defects, and so would not provide more corrosion protection. On the contrary, it reduced conductivity. Specimen 1 had the second thickest oxide film, 38.6 Å. This is verified by the results from the surface roughness measurement shown in Table 1. It can be concluded that not enough processing time was allowed for the electrochemical process to be effective. The thicknesses of the oxide film for specimens 2–4 were all around 26 Å. Judging from Fig. 3a, it may be concluded that the structure was dense and smooth. It exhibited hydrophobic property. This may be beneficial to the gas flow and water removal of a PEM fuel cell.

3.3. Electrochemical characteristics—uniform and localized corrosion analyses

Electrochemical characteristics of the oxide film were analyzed by the uniform corrosion test and pitting test. The uniform corrosion test provides a general evaluation of the corrosion rate. The pitting potential analysis provides the more critical information about localized corrosion phenomena.

3.3.1. The uniform corrosion test

The uniform corrosion test was carried out following the ASTM G5 standard [6]. The specimen was tested under room temperature with 0.5 M of H_2SO_4 solution. A Solartron 1285 potentiostat was used for the corrosion test which included a reference a electrode (REF), working electrode (WE), and an auxiliary electrode (AUX). The scanning range was between −0.5 and 0.5 V (versus SCE), and the scanning rate was 10 mV/s.

Table 4 shows the uniform corrosion rates of the specimens. For specimen 2, the uniform corrosion rate had a four-fold improvement, with a decrease from 0.1 to 0.0278 mmPy. The other specimens also showed a two- to three-fold improvement. The uniform corrosion rates were reduced to around 0.03 and 0.04 mmPy.

Specimen 2 was immersed in the H_2SO_4 solution for various periods in order to evaluate the effect of a long term corrosive environment on its corrosion resistant capability. The same uniform corrosion tests were conducted after 60, 120 and 240 h. The uniform corrosion rates were 0.028, 0.031 and 0.033 mmPy, respectively. This indicated that the oxide film from the electrochemical process was stable and solid.

3.3.2. The localized test—pitting potential analysis

A new chrome rich oxide film was formed and the uniform corrosion resistant was improved after the electrochemical process. However, the chrome rich surface increased the difference in reduction potential between chrome rich and chrome poor regions in micro scale. It would induce localized corrosion especially at corrosive environment [7]. As a result, localized corrosion is phenomenon is another corrosion behavior to be confirmed.

The Solartron 1285 potentiostat with platinum cathode and SCE reference electrode was employed for the pitting corrosion test. The reverse potentiodynamic polarization curve was used to evaluate the surface electrochemical characteristics. This test followed the ASTM G61 standard and used pitting potential and hysteresis as indicators to verify the improvement in pitting corrosion after the EP process. The test solution was 3.56% NaCl (by weight). Temperatures of the solution were 25 and 55 °C, respectively. The scanning range was between 200 and 600 mV. The scanning rate was 10 mV/s.

A typical reverse potentiodynamic polarization plot is shown in Fig. 4. The pitting potential is estimated by the intersection point of the slopes of the passivity and post-passivity states. When the potential is higher then the $E_{pit,}$ new pits will pop up. The intersection of the forward scanning and reverse scanning is referred to as the protection potential, E_{prot}. In

Table 4
Results of uniform corrosion tests

Test no.	Original specimen	Processed specimen 1	Processed specimen 2	Processed specimen 3	Processed specimen 4
Corrosion rate (mmPy)	1.0E−01	3.99E−02	2.78E−02	3.03E−02	3.82E−02
Improvement %	–	58.200	70.881	68.232	59.968

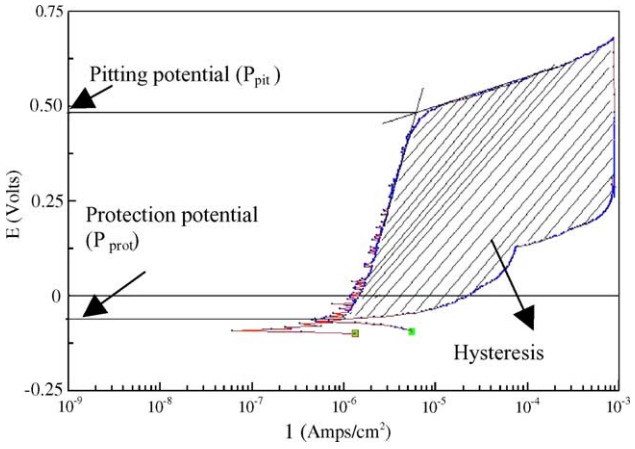

Fig. 4. Definition of pitting potential, hysteresis and protection potential.

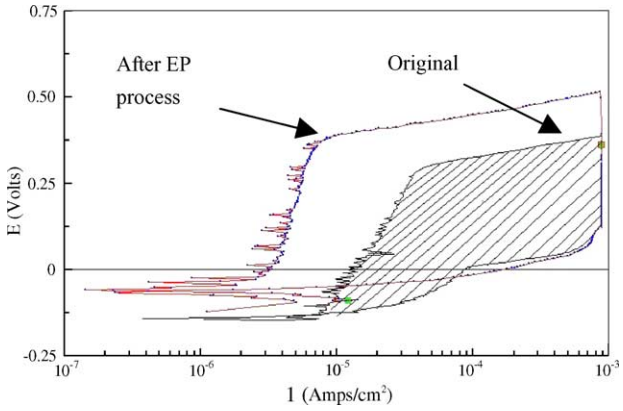

Fig. 5. Reverse potentiodynamic polarization curves of the original and the EP processed specimen.

between E_{prot} and $E_{pit,}$ new pits will not be induced. However, if there is hysteresis, the old pits may still grow. Below E_{prot}, no pitting occurs.

The hysteresis is the area enclosed by the curve. A larger hysteresis stands for a higher corrosion rate after pitting corrosion has occurred. The shaded area in Fig. 4 is the hysteresis of the original specimen. The reverse potentiodynamic polarization curves of the original and the EP processed specimen was shown in Fig. 5. Results of both of the pitting potentials and hystereses for the two testing temperatures are shown in Table 5.

The pitting potentials of the EP processed specimen, shown in Table 5, were all much higher than the original specimen. The pitting potential decreases as the temperature increases. As the temperature increases from 25 to 55 °C, the pitting potential decreases, in general, about 18%–23%. At 25 °C, the pitting potentials of the EP processed specimen were higher than that of the original specimen by approximately 16%–26%. At 55 °C, the improvements were about 26%–36% respectively. Therefore, it is evident that the electrochemical process greatly reduces the propensity for localized corrosion.

In Table 5, the electrochemical processed specimens are all higher than the original specimen in the hysteresis. This means that the electrochemical process can improve the resistance of localized corrosion but it is difficult if not impossible to prevent the growth of the defects.

The hysteresis also increases with the increase in temperature. However, the temperature effect on the electrochemical processed specimen is neither strong nor is it consistent. Therefore, it was evident that the electrochemical processed specimen had a better environmental resilience.

3.4. Contact resistance analysis

The stacking of a PEM fuel cell is a sandwich-like serial design. The macro-form (surface profile) and micro-form (surface roughness and cleanliness) of the contacting surfaces and the stacking pressure may affect the interface contact characteristics [8].

The contact resistances versus the assembly pressures of these four specimens were measured and are shown in Fig. 6. From these curves, the proper stacking pressure can be evaluated which should take into considerations of the contact resistance and the gas diffusion layer integrity in order to obtain an effective cell performance.

The results showed that the contact resistances of all of the processed specimens were lower than the original specimen. The contact resistance of specimen 2 was the lowest. This can be explained by the cleaner and thinner oxide film of

Table 5
Results of pitting potential analyses

Test no.	Original specimen	Processed specimen 1	Processed specimen 2	Processed specimen 3	Processed specimen 4
25 °C					
Pitting potential (mV)	378	446	476	437	442
Increased %	–	18	25.9	15.6	16.9
Hysteresis ($\times 10^4$)	3.16	4.70	4.65	4.53	3.78
Increased %	–	48.7	47.2	43.4	19.6
55 °C					
Pitting potential (mV)	292	398	371	374	367
Increased %	–	36.3	27.1	28.1	25.7
Hysteresis ($\times 10^4$)	3.89	4.60	4.76	4.35	4.20
Increased %	–	18.3	22.4	11.8	8

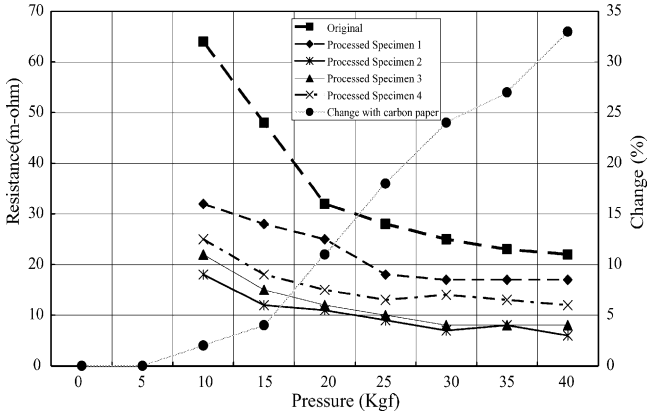

Fig. 6. Plots of contact resistance vs. stacking pressure and % thickness change of gas diffusion layer.

the processed specimens. From Table 3, the oxide film thickness of the original specimen was 47.7 Å while the values of the processed specimens were 38.6, 25.8, 26.7 and 27.8 Å, respectively. The contact resistance remained constant after 30 kgf stacking pressure.

However, the gas diffusion layer became over-compressed when the stacking pressure exceeded 30 kgf. Visible damage was observed. When the gas diffusion layer was compressed, the porosity of its micro-channels became reduced or damaged. The function of these micro-channels as a means of uniform distribution of fuels was degraded. Therefore, a compromise between contact resistance and porosity of the gas diffusion layer is inevitable. The compressed thicknesses of the gas diffusion layer are plotted in Fig. 4. Their values are presented in Table 6. Since the contact resistance did not decrease when the stacking pressure exceeded 30 kgf at the same time the gas diffusion layer was damaged, the proper stacking pressure was selected as 25 kgf.

3.5. Single cell performance and cell life tests

Single cells of graphite, the original SS316L plates and the four processed SS316L bipolar plates were assembled for cell-performance and cell-life tests. The ElectroChem testing station was employed for these tests. The fuels were pure hydrogen and pure oxygen gases. The reaction area was 25 cm^2. The in-house control interface was designed using Labview and Matlab to control gas intake flow and to record current and potential outputs.

Figs. 7 and 8 presented the *I–V* and *I–P* curves of the single cells with graphite, original SS316L and the processed SS316l (specimen 2) bipolar plates. At 0.6 V, the current densities were 600, 423 and 331 mA cm^{-2}, respectively. The

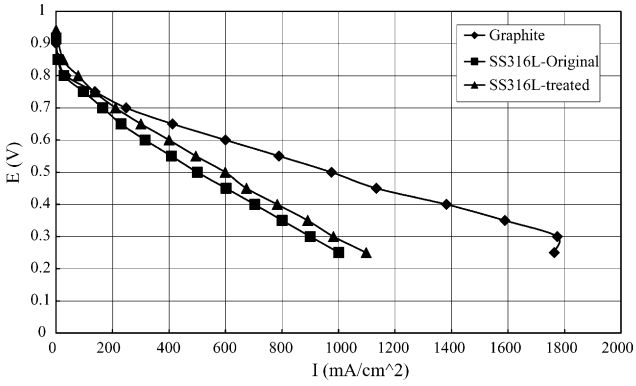

Fig. 7. *I–V* curves of graphite and SS316L single cells.

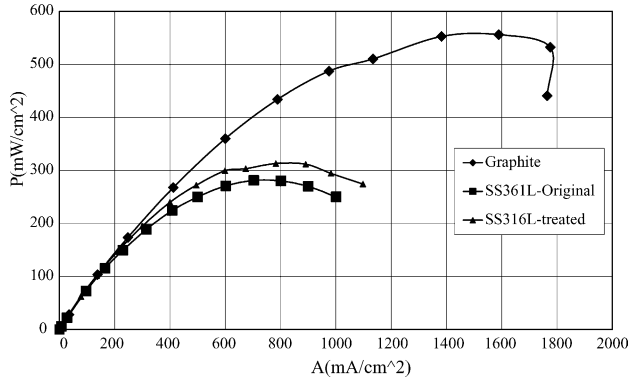

Fig. 8. *I–P* curves of graphite and SS316L single cells.

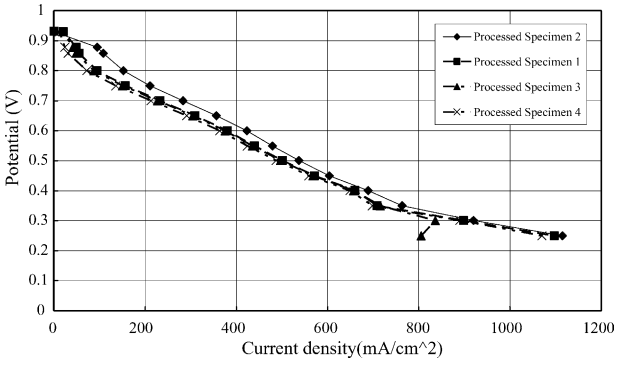

Fig. 9. *I–V* curves of single cells with processed SS316L bipolar plates.

graphite cell performed better than the SS316L cells. The processed SS316L cell performed better than the original unprocessed SS316L cell. Fig. 9 showed the *I–V* curves for all of the four processed SS316L single cells. They all had a similar performance, even though specimen 2 performed slightly better.

Table 6
Compressed thickness of gas diffusion layer

Pressure (kgf)	Original	10	15	20	25	30	35	40
Thickness (mm)	0.45	0.44	0.43	0.40	0.37	0.34	0.33	0.30
Change %	–	2	4	11	18	24	27	33

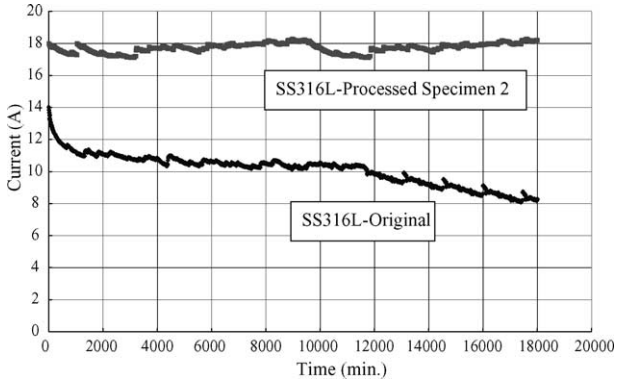

Fig. 10. 300 h cell life tests.

Fig. 10 shows the 300 h duration of cell life tests conducted for single cells with the original and the processed (specimen 2) bipolar plates. The cell with the processed bipolar plate performed steadily at 423 mA cm^{-2} through out the test duration. On the other hand, the cell performance with the original un-processed plate deteriorated continuously from 331 to 189 mA cm^{-2}. This phenomenon may have been caused by the corrosion of the oxide film. It then induces the MEA poison.

4. Conclusions

An electrochemical surface treatment process was developed for SS316L to meet the functional requirements of the bipolar plates of PEM fuel cells. Four test specimens with different process parameters were prepared. The processed specimen had brighter and smoother surface. Two corrosion tests, uniform and pitting potential analyses, were conducted to verify the significant improvement in corrosion resistant characteristics of the processed specimens. The ESCA spectrum showed that the chemical composition of the oxide film had become enriched with Cr after the process, and this was the main reason for the improved corrosion resistance. The AES depth profile also indicated that the thickness of the oxide film was much less then the original. The thinner and denser oxide film leads to reduction in both surface and contact resistance. The 300 h of cell life tests showed that the single cell with the processed bipolar plate had consistent cell performance which may indicate much reduced metallic ion poison to the MEA.

Therefore, the proposed surface treatment process greatly improves the surface integrity of SS316L stainless. This will allow stainless steel to be a good potential metallic material for use in PEM fuel cells.

Acknowledgements

This research is funded by Ministry of Economic Affairs, Taiwan 91-EC-17-A-05-S1-0012. The support from Yuan Ze fuel cell center is also greatly appreciated.

References

[1] R. Hornung, G. Kappelt, Bipolar plate materials development using Fe-based alloys for solid polymer fuel cells, J. Power Sources 72 (1998) 20–21.
[2] D.P. Davies, P.L. Adcock, M. Turpin, S.J. Rowen, Stainless steel as a bipolar plate material for solid polymer fuel cells, J. Power Sources (2000).
[3] H. Wang, M.A. Sweikart, J.A. Turner, Stainless steel as a bipolar plate material for polymer electrolyte membrane fuel cells, J. Power Sources 115 (2003) 243–251.
[4] S.J. Lee, J.J. Lai, The effects of electro-polishing (EP) process parameters on corrosion resistance of 316L stainless steel, J. Mater. Process. Technol. 140 (2003) 206–210.
[5] J.F. Moulder, W.F. Stickle, P.E. Sobol, K.D. Bomben, Handbook of X-ray Photoelectron Spectroscopy, Phys. Electron. (1995).
[6] ASTM G5-94, Standard Reference Test Method for Marking Potentiostatic and Potentiodynamic Anodic Polarization Measurements.
[7] J. Beddoes, K. Bucci, The influence of surface condition on the localized corrosion of 316L stainless steel orthopedic implants, J. Mater. Sci.: Mater. Med. 10 (1999) 389–394.
[8] J. Ihonen, F. Jaouen, G. Lindbergh, G. Sundholm, A novel polymer electrolyte fuel cell for laboratory investigation and in-situ contact resistance measurements, Electrochem. Acta 46 (2001) 2889–2911.